Composites Science and Technology 70 (2010) 1838–1846

Contents lists available at ScienceDirect

Composites Science and Technology

journal homepage: www.elsevier.com/locate/compscitech

Novel 3D porous multi-phase composite scaffolds based on PCL, thermoplastic zein and ha prepared via supercritical CO_2 foaming for bone regeneration

Aurelio Salerno [a,b,*], Stefania Zeppetelli [b], Ernesto Di Maio [c], Salvatore Iannace [b], Paolo A. Netti [a,c]

[a] Interdisciplinary Research Centre on Biomaterials (CRIB) and Italian Institute of Technology (IIT), Piazz.le Tecchio 80, 80125 Naples, Italy
[b] Institute of Composite and Biomedical Materials, National Research Council (IMCB-CNR), Piazz.le Tecchio 80, 80125 Naples, Italy
[c] Department of Materials and Production Engineering (DIMP), University of Naples Federico II, Piazz.le Tecchio 80, 80125 Naples, Italy

ARTICLE INFO

Article history:
Available online 25 June 2010

Keywords:
A. Functional composite
B. Mechanical properties
D. Scanning electron microscopy
Bone scaffold

ABSTRACT

The aim of this study was the design of novel biodegradable porous scaffolds for bone tissue engineering (bTE) via supercritical CO_2 ($scCO_2$) foaming process. The porous scaffolds were prepared from a poly(ε-caprolactone)-thermoplastic zein multi-phase blend w/o interdispersed hydroxyapatite particles (HA) and the porous structure achieved via the $scCO_2$ foaming technology. The control of scaffolds porosity was obtained by modulating materials formulation and foaming temperature (T_F). The scaffolds were subjected to morphological, micro-structural and biodegradation analyses, as well as *in vitro* biocompatibility tests. Results demonstrated that both HA concentration and T_F significantly affected the micro-structural features of the scaffolds. In particular, scaffolds with porosity and pore size distribution, mechanical properties and biodegradability adequate for bTE were designed and produced by selecting a T_F equal to 100 °C for all the compositions used. The biocompatibility of these scaffolds was assessed *in vitro* by using osteoblast-like MG63 and human mesenchymal stem cells (hMSCs).

1. Introduction

The recent developments in bone tissue engineering (bTE) in understanding the cell-scaffold interactions as well as the development of technologies for the production and characterization of porous scaffolds allowed the birth of "third-generation" biomaterial scaffolds: bioactive and biodegradable scaffolds designed to provide a temporary 3D micro-environment for cells and tissues and, simultaneously, to guide cellular processes involved in de novo tissue genesis [1–3]. To achieve these aims, a bTE scaffold must: (i) provide an optimal pore structure and an adequate mechanical stiffness; (ii) constitute a temporary structure with degradation and resorption rates matching the growth of the new bone tissue, *in vitro* or *in vivo*; (iii) elicit specific interactions with cells, promoting cell adhesion, proliferation and biosynthesis [1–3].

First of all, it has been proved that an interconnected pore-structure with pore size in the 100–500 μm range is necessary to promote cells adhesion, proliferation and three-dimensional colonization, as well as to enhance fluid diffusion within the 3D cell/scaffold construct [2,4–6]. On the other hand, providing adequate mechanical support, such as a compression modulus higher than 10 MPa in the case of bone scaffold, is a critical *in vivo* requirement to avoid excessive neo-tissue deformation under physiological loadings [7]. It is also a requirement that scaffold degradation and resorption rates have to be controlled accurately. For instance, in the case of bTE, the biodegradable scaffold must retains its structural properties for several months [1]. Finally, biomaterial scaffolds must be capable of promoting cell adhesion, proliferation and differentiation, as well as extracellular matrix deposition [1–3].

Several approaches have been used in bTE to produce scaffolds with tailored micro-structural properties and biological response. From the materials side, hybrid composite materials prepared by mixing biocompatible and biodegradable polymers with osteoinductive ceramic particles, such as hydroxyapatite (HA), allowed the design of scaffolds characterized by optimal micro-structural properties, tailored biodegradation rates and, in some cases, enhanced cell adhesion and biosynthesis if compared to neat materials [1–3,8–12]. Multi-phase polymer blends prepared by mixing synthetic and natural polymers were successfully prepared to enhance the control over scaffold degradation and hydrophilicity [13,14]. For instance, Rosa et al. reported that the degradation rate of poly(ε-caprolactone) (PCL) was accelerated after blending with starch and, the extent of degradation increased with increasing starch content [14]. Among the natural polymeric materials, zein, a major storage protein of corn, was recently used for the design of bTE scaffolds [10,15]. These scaffolds allowed for the adhesion, proliferation and osteogenic differentiation of human mesenchymal stem cells (hMSCs) *in vitro*, as well as for new-bone regeneration guided by MSCs *in vivo* [10,15].

* Corresponding author at: Interdisciplinary Research Centre on Biomaterials (CRIB) and Italian Institute of Technology (IIT), Piazz.le Tecchio 80, 80125 Naples, Italy. Fax: +39 0817682404.
E-mail address: asalerno@unina.it (A. Salerno).

0266-3538/$ - see front matter © 2010 Elsevier Ltd. All rights reserved.
doi:10.1016/j.compscitech.2010.06.014

Recently, supercritical CO_2 ($scCO_2$) foaming has achieved great interest in tissue engineering for the possibility to designing porous scaffolds with well controlled pore structure, without the use of organic solvents potentially harmful for cells and biological tissues [16,17]. Furthermore, the low $scCO_2$ temperature and pressure (31.1 °C and 73.8 MPa, respectively) allowed for the design of drug delivery systems and bioactive tissue engineering scaffolds, as well as to produce 3D cell/scaffold constructs in a single step process [18,19].

We recently investigated the foaming process of multi-phase PCL blends with the aim of designing PCL scaffolds with well controlled pore structures [20]. Along with this research line, this work reported the design and fabrication of novel multi-phase scaffolds for bTE by $scCO_2$ foaming. The scaffolds were prepared by blending PCL with thermoplastic zein (TZ), a thermoplastic material obtained by mixing zein with poly(ethylene glycol) (PEG) [21]. Furthermore, HA particles, in concentration of 10 wt.% and 20 wt.%, were added to the PCL–TZ blend for the preparation of multi-phase composites. The as prepared systems were subsequently processed via $scCO_2$ foaming to design 3D porous scaffolds. The effect of HA concentration and foaming temperature (T_F) on the pore structure of the scaffolds was investigated, finally aiming to prepare 3D porous scaffolds for bTE. The selected scaffolds were further tested in order to characterize their mechanical properties, *in vitro* degradation and biocompatibility.

2. Experimental

2.1. Materials

PCL (M_W = 65 kDa, T_m = 59–64 °C, T_g = −60 °C, and ρ = 1.145 g/cm^3) and maize zein powder (cod.: Z3625, batch: 065K0110) were purchased from Sigma–Aldrich (Italy). PEG 400 was purchased from Fluka (Italy) and used as plasticizer for the preparation of the TZ. Porous HA particles (Fin-Granule, Finceramica, Faenza, Italy) with size in the 70–105 μm range, were used as bioceramic filler.

2.2. Methods

The TZ was prepared as described in a previously reported work [21]. Briefly, the "as received" zein powder was pre-mixed with PEG 400 in a beaker (4:1 mass ratio, respectively) and then fed into a twin counter rotating internal mixer (Rheomix 600 Haake, Germany) connected to a control unit (Rheocord 9000 Haake, Germany) for thermoplasticization. Mixing conditions were: 80 °C, 50 rpm and 10 min. The TZ was then extracted from the mixer and manually formed into small pellets for further processing.

For multi-phase biomaterials preparation, PCL pellets were first melted at 70 °C, 20 rpm for 2 min and subsequently TZ and HA granules were added into the mixing chamber and mixed at 70 °C, 80 rpm for 6 min. Table 1 reports the three different compositions and adopted classification. Finally, the compounds were compression molded at 80 °C and 30 MPa into 2 mm-thick plates by a hot press (P300P, Collin, Germany).

Foaming experiments were carried out on disc-shaped samples (d = 10 mm and h = 2 mm). The samples were solubilized with CO_2 for 4 h at 70 °C and 150 MPa and subsequently rapidly cooled or heated to the desired T_F (in the 44–100 °C range) with a controlled temperature profile. The pressure was finally quenched to the atmosphere at a pressure drop rate of 700 bar/s allowing samples foaming. To stabilize the pore structure, foams were immediately cooled down to ambient temperature and removed from the vessel.

Table 1
Composition of the different systems prepared.

Sample	PCL (wt.%)	TZ (wt.%)	HA (wt.%)
PCL–TZ	60	40	0
PCL–TZ–HA_{10}	54	36	10
PCL–TZ–HA_{20}	48	32	20

2.3. Characterization

The thermal degradation of the biomaterials was investigated by thermogravimetric (TGA) and derivative TGA (DTGA) analyses. The tests were carried out on a TGA2950 (TA Instruments, USA) over a 30–600 °C temperature range at 10 °C/min under inert atmosphere. Neat PCL and TZ were also tested for comparison.

The morphology of the scaffolds was assessed by Scanning Electron Microscope (SEM, LEICA S440) analysis.

The porosity of the scaffolds was determined from the mass and the volume measurements by using the following equation:

$$\%\text{porosity} = \left[1 - \left(\frac{\rho_S}{\rho_M}\right)\right] \times 100$$

where ρ_S and ρ_M are the apparent densities of the scaffolds and biomaterials, respectively, calculated as the mass to volume ratio on cylindrical samples. The mass was measured by using a high accuracy balance (10^{-3} g, AB104-S, Mettler Toledo, Italy) while the volume determined by geometrical calculation using a high precision caliper. Three different measurements were performed for each scaffold type. Pore size was calculated by image analysis, according to ASTM D3576. In particular, the SEM micrographs were converted to binary images and analyzed by Image J® software in order to evaluate the pore size distribution and the mean pore size of the scaffolds. At least 100 pores were analyzed for each scaffolds formulation.

The compressive mechanical properties of the scaffolds were evaluated by an Instron 4204 (Instron, Italy) equipped with a 1 kN loading cell and working at 1 mm/min cross head velocity. The elastic compression modulus (E) was determined as the slope of the initial linear portion of the stress (σ) vs. strain (ε) curve, while the compression yield strength (σ_Y) and strain (ε_Y) were calculated with the modulus slope at 1% strain offset. Five cylindrical samples (d = 5 mm and h = 5 mm) were tested for each formulation.

The scaffolds were γ-sterilized and subjected to *in vitro* degradation and biocompatibility tests. For the degradation study, the scaffolds were soaked in double distilled water at 37 °C for 21 days. At pre-determined time points, the scaffolds were washed with fresh water, dried and analyzed by SEM for morphological characterization and by gravimetric measurements to assess the weight loss. The weight loss was determined as the percent ratio between the final and the initial scaffold weights.

The biocompatibility of the scaffolds was assessed by using two different cell lines: MG63 and hMSCs cells. For the MG63 *in vitro* test, the cells (kindly provided by Prof. R. Quarto, University of Genoa, Genoa, Italy) were cultured in 75-cm^2 flask at 37 °C in humidified incubator with 5% CO_2, washed with phosphate-buffered saline (PBS) and incubated with trypsin–EDTA (0.25% trypsin, 1 mM EDTA, Euroclone) for 5 min at 37 °C. Subsequently, 10,000 cells, resuspended in 50 μL of medium, were seeded onto the scaffolds (d = 5 mm, h = 5 mm), following incubation for 2 h in 24-well culture plates to allow for cell adhesion. Cell culture medium was then added to each well to bring the total volume to 1.5 mL. Culture medium used was Dulbecco's modified Eagle's medium supplemented with 10% fetal calf serum (Gibco-BRL Life Technologies, Italy) and antibiotics (penicillin G sodium 100 U/mL, streptomycin 100 μg/mL, Euroclone). After 1 day of

incubation, the cell/scaffold constructs were removed from the media, washed with PBS and fixed with 2.5% glutaraldehyde (Sigma–Aldrich, Italy) in 0.1 M Na-cacodylate (Carlo Erba, Italy) at pH 7.4. The cell/scaffold constructs were then freeze-dried overnight and analyzed by SEM.

For the hMSCs experiments, the cells were incubated at 37 °C for 60 min in PBS containing 25 μM of green 5-chloromethyl-fluorescein diacetate (CMFDA, Molecular Probes, USA), followed by 10% fetal bovine serum DMEM for an additional 2 h. The cells were washed twice with PBS to remove the exceeding dye, seeded onto the scaffold (20,000 cells/scaffold) and cultured *in vitro* for 1 day. hMSCs adhesion and distribution were investigated by Confocal Laser Scanning Microscopy (CLSM, 510, Zeiss, Germany) using a 10× objective.

2.4. Statistical analysis

The statistical significance of the results was assessed by one-way ANOVA. Tukey post hoc test at the significance level $p < 0.05$ was used to identify statistically different data by using Origin® software package.

3. Results and discussion

3.1. Biomaterials preparation and characterization

Fig. 1 reports torque and temperature histories during the mixing process of PCL–TZ and PCL–TZ–HA_{20}. For both the systems we observed that torque attains a maximum in the early stages of mixing and subsequently decreases to a rather stationary value, when also the melt temperature becomes quite constant. Similar trends were reported for melt blending processes of others thermoplastic polymers and fillers, indicating the achievement of uniform dispersions between polymers and HA particles [20,22]. Furthermore, as evidenced in Fig. 1, the temperature evolution during the preparation of PCL–TZ–HA_{20} composite was characterized by higher values, with respect to PCL–TZ, probably due to the enhanced dissipative effect caused by the inorganic particles during the melt-mixing process.

Fig. 2a and b shows the TGA and DTGA curves, respectively, for the different multi-phase systems, as well as those of neat PCL and TZ. Table 2 provides the details of the degradation temperatures and residual weights based on the TGA and DTGA thermograms.

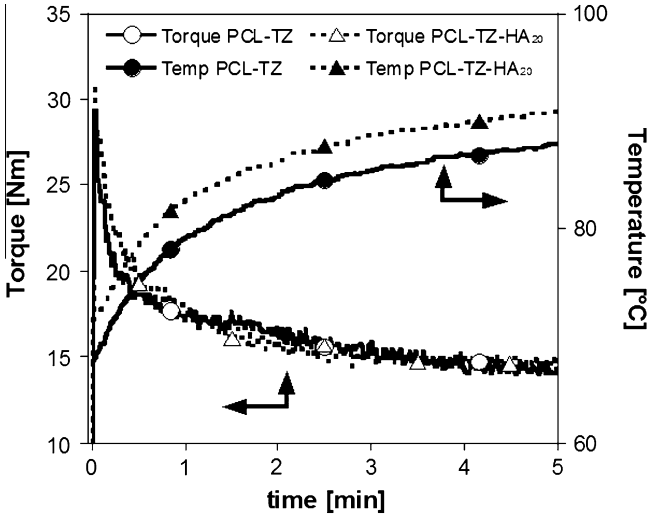

Fig. 1. Torque (open symbols) and melt temperature (closed symbols) evolution during the melt-mixing process used for the preparation of PCL–TZ (circles) and PCL–TZ–HA_{20} (triangles) systems.

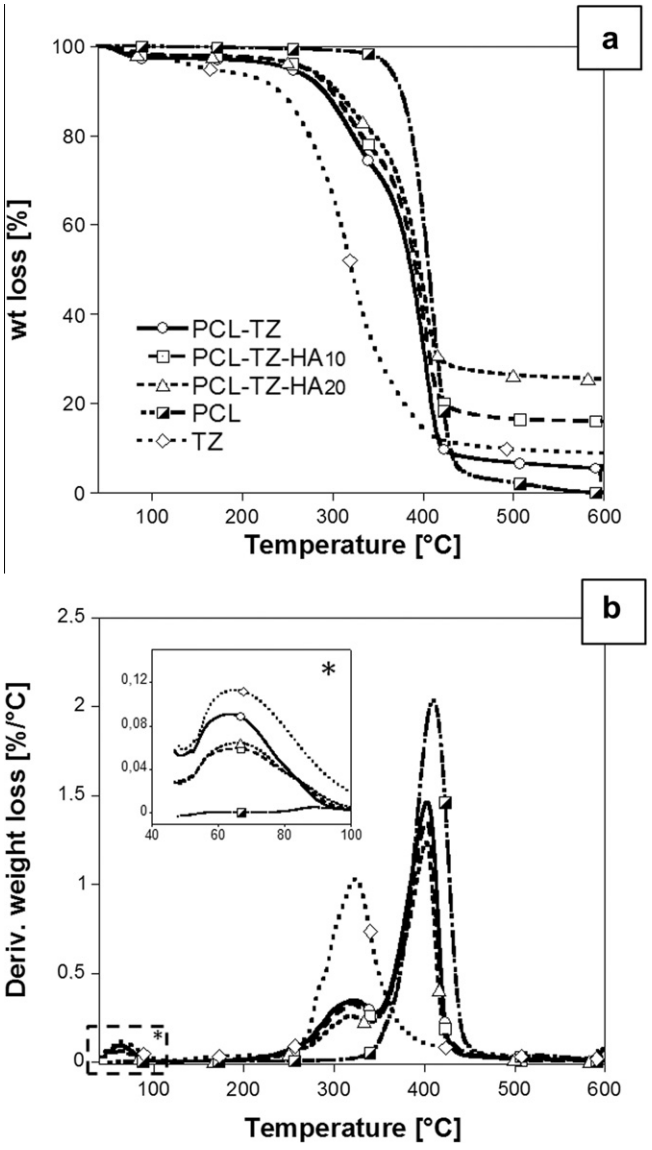

Fig. 2. (a) TGA and (b) DTGA curves of the different multi-phase systems prepared. Neat PCL and TZ are also reported for comparison.

DTGA curve of PCL–TZ showed three peaks. The first peak in the 40–100 °C range (inset of Fig. 2b) may be attributed to the evaporation of the water and low molecular weight compounds, such as PEG molecules, from the TZ phase. The second and third peaks, at 321.4 and 403.5 °C, can be attributed to the thermal degradation of TZ and PCL, respectively (Fig. 2 and Table 2). These results proved the heterogeneous nature of the systems prepared. The addition of HA slightly decreased the thermal stability of PCL (Peak III decreased from 409.8 °C for neat PCL to 402.2 °C for PCL–TZ–HA_{20}), with a residual weight at 600 °C equal to 16% for PCL–TZ–HA_{10} and equal to 25.4% for PCL–TZ–HA_{20} (Fig. 2a and Table 2). Furthermore, PCL degraded completely at the final test temperature, while for neat TZ we observed a final residue equal to 8.8% (Table 2). The presence of a residual mass at temperatures higher than 450 °C was also reported by Sessa et al. for melt-processed corn zein [23] and by Mariani et al. for corn starch blends [24] and, has been ascribed to inorganic compounds derived from thermal degradation [23,24]. By considering the material formulations used (Table 1) and the TGA results (Table 2), we may conclude that the final residues of PCL–TZ–HA_{10} and PCL–TZ–HA_{20} at 600 °C well matched the nominal HA amount within the composites.

Table 2
Thermal degradation and residual weight at 600 °C of the multi-phase systems. Neat PCL and TZ are also reported for comparison.

Sample	Peak I (°C)	Peak II (°C)	Peak III (°C)	Residue at 600 °C (wt.%)
PCL	–	–	409.8	–
TZ	65.1	323.9	–	8.8
PCL–TZ	63.3	321.4	403.5	5.2
PCL–TZ–HA_{10}	64.9	321.1	402.5	16
PCL–TZ–HA_{20}	65.6	317.7	402.2	25.4

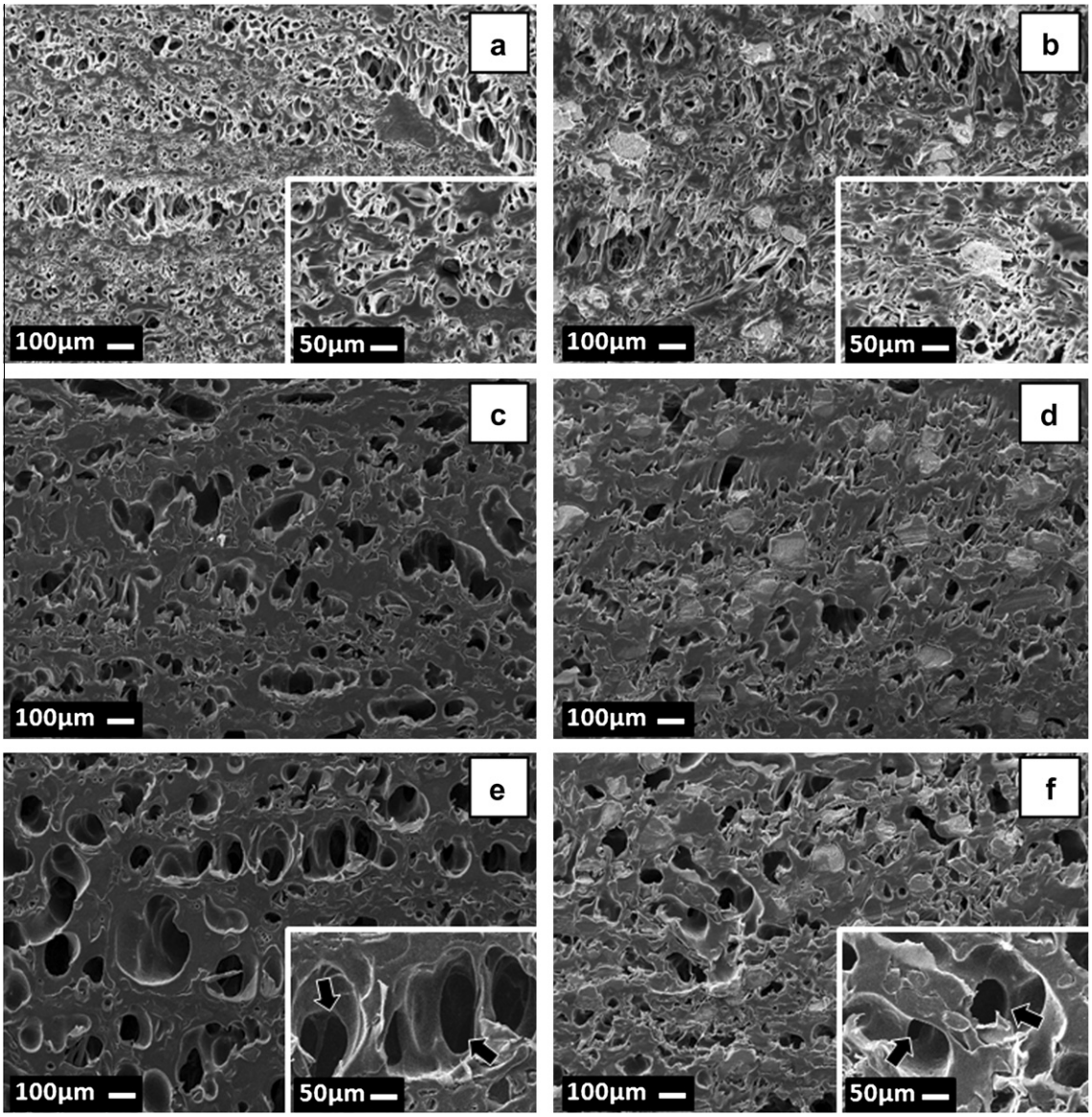

Fig. 3. Effect of T_F on the morphology of the PCL–TZ (a, c, e) and PCL–TZ–HA_{20} (b, d, f) scaffolds: (a and b) T_F = 44 °C; (c and d) T_F = 80 °C; (e and f) T_F = 100 °C. The insets show higher magnifications SEM micrographs of the PCL–TZ and PCL–TZ–HA_{20} scaffolds, respectively, evidencing pores morphology and interconnectivity (black arrows of Figures 3e and f).

3.2. Scaffold design by $scCO_2$ foaming: effect of biomaterials formulation and T_F on the morphology, porosity and pore size distribution of the scaffolds

In the past few years, gas foaming process has emerged as a very promising tool for the design of tissue engineering scaffolds with fine controlled pore structures [2,16,17]. Indeed, this technique allowed the control over the micro-architecture of the pore structure of the scaffolds by the appropriate selection of the processing parameters, mainly blowing agent type (e.g. CO_2, N_2 or their mixtures), T_F, saturation pressure and pressure drop rate [16,17]. Furthermore, with the addition and subsequent removal of a porogen agent, enhanced tuning of the micro-architecture of the pore structure of the scaffold has been achieved [11,20,25,26].

By considering the main importance of T_F on the final properties of porous material prepared via the gas foaming process [21,25–27], we limited our investigation on the effect of different T_F on the final morphology, porosity and pore size distribution of the

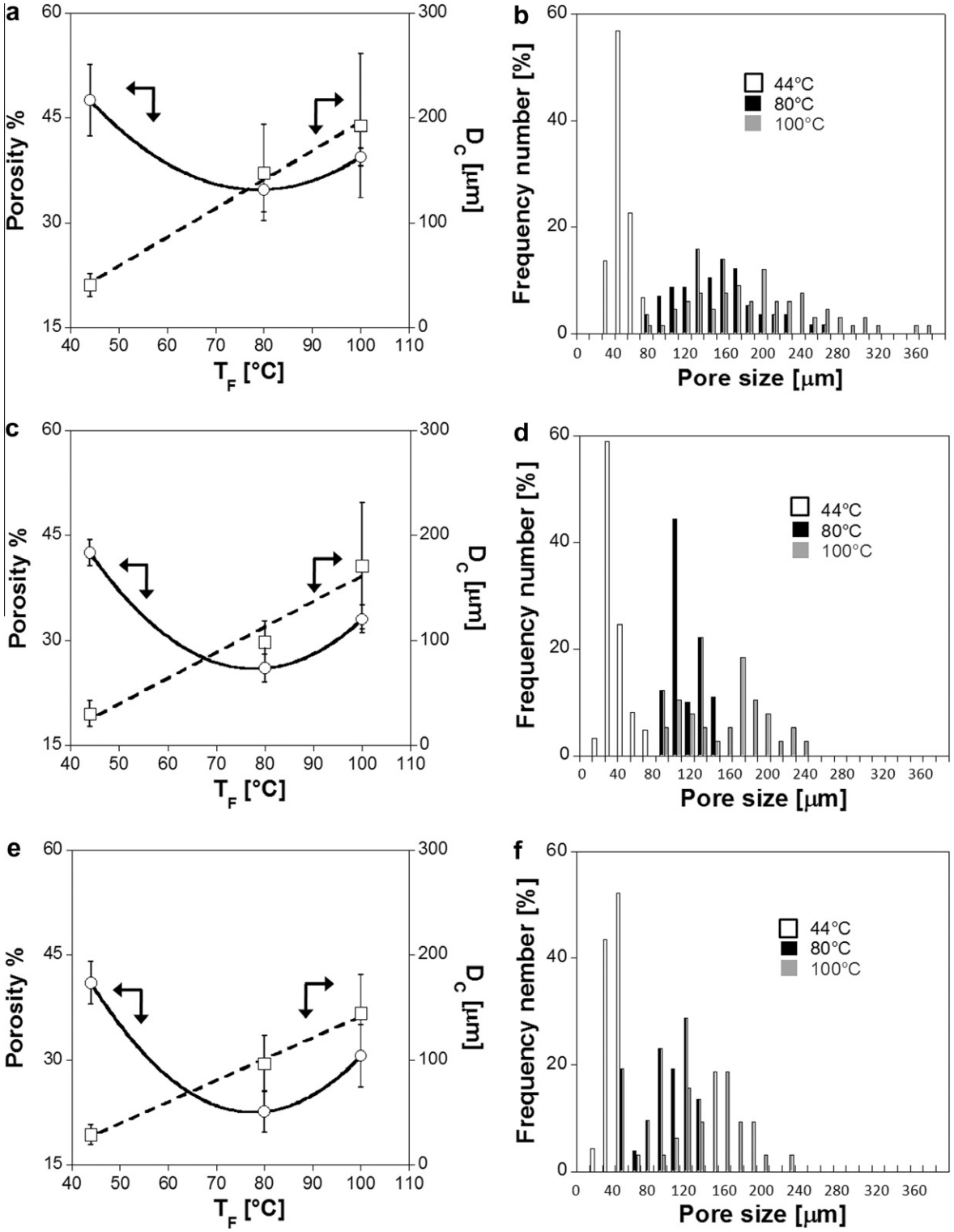

Fig. 4. Effect of T_F on the porosity, D_C and pore size distribution of the scaffolds: (a and b) PCL–TZ; (c and d) PCL–TZ–HA_{10}; (e and f) PCL–TZ–HA_{20}. The porosity values represent the mean ± standard deviation of three different measurements ($p < 0.05$).

scaffolds. Other processing parameters have been fixed as: saturation pressure equal to 150 MPa and pressure drop rate equal to 700 bar/s. This selection allowed the achievement of properly expanded systems and was based on previous works on multiphase systems [20,25].

Fig. 3 reports the morphology of the PCL–TZ and PCL–TZ–HA_{20} composite scaffolds prepared by selecting different T_F, showing that the pore structure changed drastically for T_F lying below or above PCL melting temperature (T_m = 59–64 °C). Indeed, at T_F = 44 °C (below T_m), a small porosity was achieved into the PCL phase, as a consequence of PCL crystallization during bubbles growth (Fig. 3a and b). The PCL–TZ–HA_{20} composite was characterized, hence, by smaller pores (compare the high magnification insets reported in Fig. 3a and b), mainly because of the enhanced

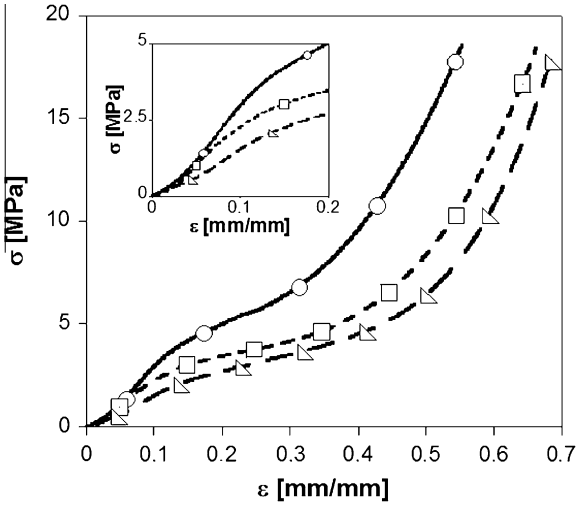

Fig. 5. Representative σ–ε curves obtained by the static compression tests of PCL–TZ (triangles), PCL–TZ–HA_{10} (squares) and PCL–TZ–HA_{20} (circles) scaffolds prepared at T_F = 100 °C. The inset shows a higher magnification of the elastic region.

Table 3
Static compression properties of the porous scaffolds prepared at T_F = 100 °C.

Sample	E (MPa)	ε_Y (mm/mm)	σ_Y (MPa)
PCL–TZ	18.1 ± 1.1	0.14 ± 0.04	2.19 ± 0.1
PCL–TZ–HA_{10}	29.2 ± 2.1	0.12 ± 0.04	2.49 ± 0.7
PCL–TZ–HA_{20}	32.4 ± 2.5	0.103 ± 0.01	3.39 ± 0.7

stiffness of the polymeric matrix [27,28]. Conversely, by performing foaming at $T_F > T_m$, the pores that nucleated into the PCL phase coalesced before the crystallization of the polymeric matrix, resulting in the formation of bigger, collapsed PCL pores at the PCL–TZ interface (Fig. 3c–f). Furthermore, we observed the increase of the pore size when T_F increased from 80 °C (Fig. 3c and d) to 100 °C (Fig. 3e and f), as a consequence of the further decrease of the stiffness of the two polymers [27,28]. The higher magnifications of the PCL–TZ and PCL–TZ–HA_{20} composite scaffolds prepared at T_F = 100 °C, reported in the insets of Fig. 3e and f, respectively, also showed the presence of pore interconnectivity (black arrows). Looking at the TZ phase, a smaller porosity was observed (not shown), due to the higher stiffness of this polymer, with respect to the PCL [21]. It is also important to point out that all of the T_F selected for the design of the scaffolds were significantly lower than the degradation temperature of TZ (323.9 °C, Fig. 2 and Table 2) and, therefore, the foaming experiments should allow for the preservation of the chemical structure of the thermoplasticized protein.

The results of the porosity, mean pore size (D_C) and pore size distribution as a function of T_F are shown in Fig. 4. The overall porosity of PCL–TZ scaffolds decreased from 47.5% to 35.3%, when T_F increased from 44 °C to 70 °C (Fig. 4a), as a consequence of the collapse, at higher temperatures, of the pores nucleated within the PCL phase, as previously discussed. Furthermore, the porosity slight increased to 39.5% when T_F increased to 100 °C. Conversely, D_C increased from 40 μm to 200 μm when T_F increased from 44 °C to 100 °C, respectively (Fig. 4a), as well as broader pore size distributions were observed at higher T_F values (Fig. 4b). As shown in Fig. 4c–f, similar results were achieved for PCL–TZ–HA_{10} and PCL–TZ–HA_{20} composite scaffolds. Nevertheless, when compared to the PCL–TZ scaffolds, quite lower overall porosities were observed for both the composites, this reduction being more evident in the samples with the higher HA concentration. We also observed a minor decrease of D_C by increasing the HA amount from 0 wt.% to

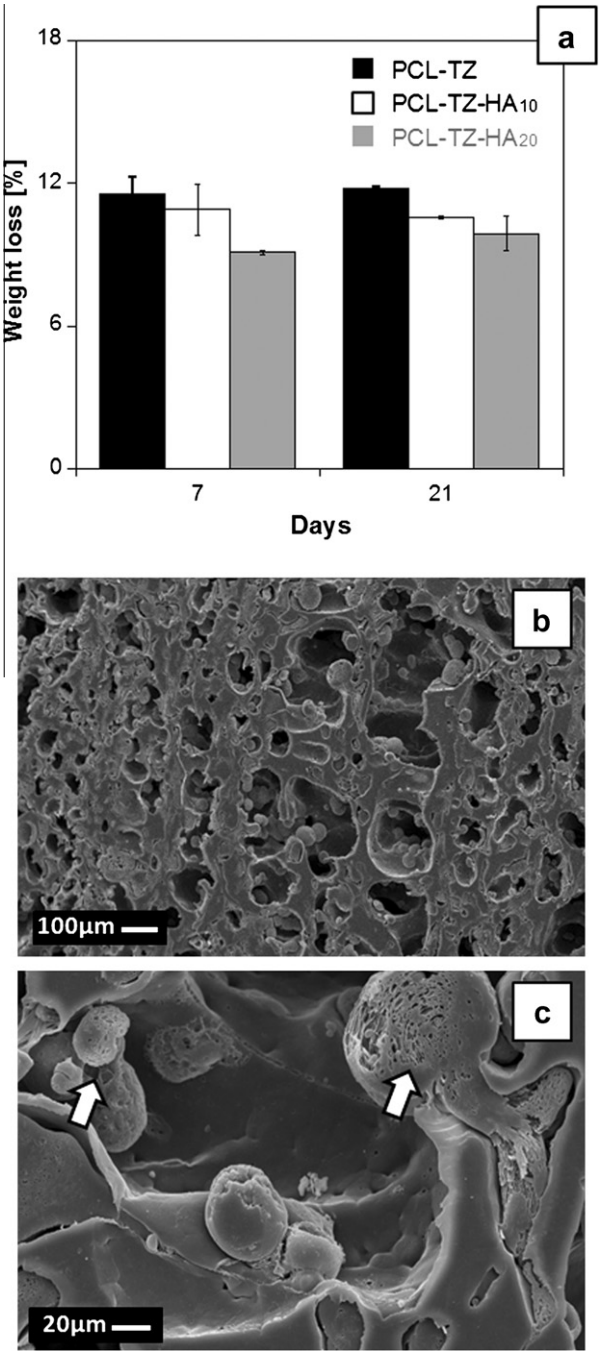

Fig. 6. (a) Weight loss of the different scaffolds after 7 and 21 days of degradation in water at 37 °C. Lower (a) and higher (b) SEM micrographs of the cross-section of the PCL–TZ scaffold after 21 days of degradation. The arrows indicate the tiny pores induced by the degradation of the TZ.

20 wt.% (compare Fig. 4a, c and e) and the shift of the pore size distribution to lower values, as shown in Fig. 4d and f. The observed pore structure differences may be ascribed to the effect of the HA on the micro-structure and foaming of the polymer blend. For instance, several studies reported that, parameters such as filler size and concentration have a strong impact on the morphology, porosity and pore size distribution of porous materials prepared by CO_2 foaming [27,28]. In our previously reported work, we showed that, by increasing the amount of NaCl particles (5 μm in size) within PCL, it was possible to obtain PCL foams characterized by a lower mean pores size and a narrower pore size distribution [27]. This effect was demonstrated to be dependent on the enhanced

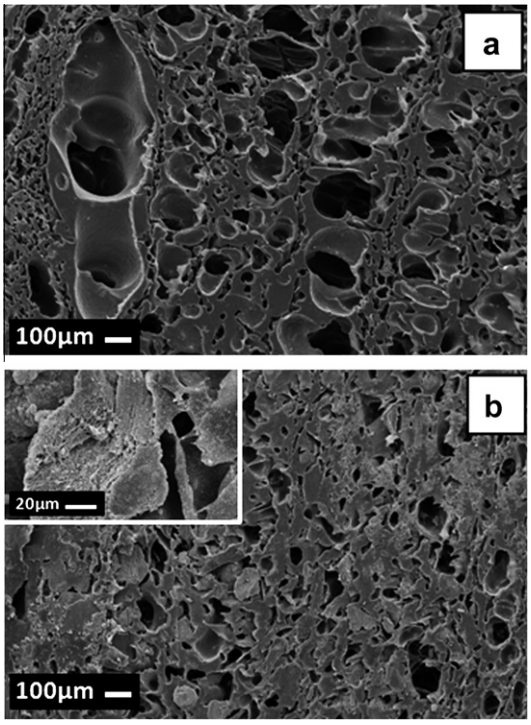

Fig. 7. SEM micrographs of: (a) PCL–TZ and (b) PCL–TZ–HA_{20} scaffolds after the selective extraction of the TZ.

stiffness of the polymeric matrix that limits gas bubbles growth and on the nucleating effect of the filler [27]. Similar results have been also achieved by Collins et al. for polylactide/silica composites prepared by using 125–250 μm silica particles [28]. It is however important to point out that the results of the pore size distribution analysis showed that the multi-phase scaffolds prepared at T_F = 100 °C were characterized by 100–200 μm pore size fractions (Fig. 4b, d and f), well matching the optimal pore size indicated for bone tissue replacement/regeneration [2,4–6]. Taking into account these results, we selected these scaffolds for further characterizations.

3.3. Mechanical properties, in vitro degradation and biocompatibility of the selected scaffolds

Providing an adequate mechanical support is a critical bTE scaffold design requirement. Indeed, the mechanical properties of the scaffold may directly affect cell behavior and biosynthesis but also define suitable *in vitro* and/or *in vivo* applications [1–3,7]. Fig. 5 reports the σ vs. ε curves of the scaffolds as a function of the HA concentration. We observed the typical trend of porous materials undergoing static compression tests characterized by an initial linear-elastic region, followed by a plateau and by the steep increase in the σ values as a consequence of the densification [29]. As shown in Fig. 5, the mechanical properties of the scaffolds under investigation increased with the increase of the HA content. In particular, E and σ_Y increased from 18.1 ± 1.1 MPa and 2.2 ± 0.1 MPa for the PCL–TZ scaffold to 32.4 ± 2.5 MPa and 3.4 ± 0.7 MPa for the PCL–TZ–HA_{20}, respectively (Table 3). This effect may be ascribed to several factors, mainly the observed decrease of the overall porosity and pore size distribution of the scaffold (Fig. 4) and the strengthening induced by the ceramic filler [30]. In the case of load-bearing tissues, such as bone, a porous scaffold must provide sufficient temporary mechanical support to withstand *in vivo* stresses and loading and to avoid excessive new-tissue deformation [1,7]. The mechanical response of the scaffolds prepared at T_F = 100 °C, characterized by E values higher than 10 MPa, well match the mechanical requirements for bTE applications [7].

The effect of the degradation, as observable by the morphology and weight loss of the scaffolds, is reported in Fig. 6. The weight loss of the scaffolds was significantly affected by their formulation, while a negligible effect was observed from day 7 to day 21 of degradation. In particular, the weight loss decreased from 11.6 ± 0.7% for the PCL–TZ scaffold to 9.1 ± 0.1% for the PCL–TZ–HA_{20} scaffold, this difference remaining almost constant at day 21 (Fig. 6a). The observed degradation is directly dependent on the multi-phase nature of the scaffolds. In effect, PCL is not susceptible to mass loss in water in the first 21 days of degradation, while zein (much more hydrophilic) is characterized by enhanced solubilization in aqueous environment [9,10]. For instance, Yao et al. reported a significant weight loss (up to 20%) for electrospun zein membranes after 4 weeks of *in vitro* degradation in PBS [31]. It is important to point out that, when thermo-plasticized with PEG, the ability of zein to swell and partially dissolve in water may be enhanced as a consequence of the lubricant effect of PEG and due to the high hydrophilic nature and solubility of the plasticizer in water. This consideration was also supported by the analysis of the weight loss at day 7 and day 21 of degradation, that were close to the nominal amount of plasticizer within the different scaffolds (Table 1). The SEM analysis of the cross-section of the PCL–TZ scaffolds after 21 days of degradation are reported in Fig. 6b and c. By comparing the morphology of the PCL–TZ scaffold before (Fig. 3e) and after 21 days of degradation (Fig. 6b and c) it was possible to detect

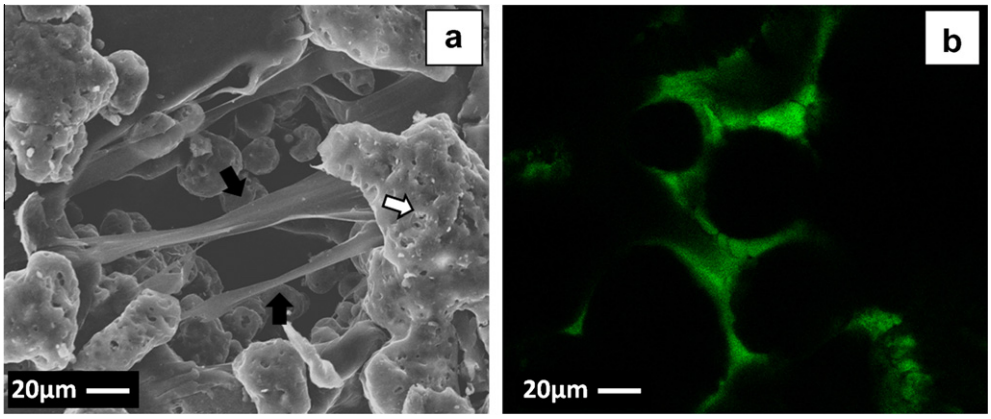

Fig. 8. (a) SEM micrograph of MG63 seeded onto the PCL–TZ scaffold at day 1 of *in vitro* culture (the black arrows indicate the MG63 cells, while the white arrow evidences the TZ phase); (b) CLSM image of the hMSCs seeded onto the PCL–TZ scaffold at day 1 of *in vitro* culture.

a more irregular and discontinuous zein network within the degraded scaffolds. Furthermore, the higher magnifications of Fig. 6c revealed the formation of a very tiny pore structure within the TZ phase, corroborating the key role of TZ on the faster degradation of the scaffolds, as previously discussed. The reported results are in agreement with the papers dealing with blending natural polymers, such as chitosan and starch, with PCL, to prepare scaffolds with enhanced hydrophilicity and faster degradation rate [13,14]. These results are very important in the perspective of using such scaffolds for bTE, with the accurate design of their micro-structural properties and degradation. Indeed, even if the "as prepared" scaffolds were characterized by quite low overall porosity degrees (40% approximately, Fig. 4), the rather fast TZ degradation may allow for the progressive increase of the pore fraction available for cell colonization and tissue infiltration. Concomitantly, the slower resorption of PCL guarantees the presence of a structural support until the tissue engineered transplant is fully remodeled by the host tissue and can assume its own structural role [1].

Fig. 7 showed the morphology of the PCL–TZ and PCL–TZ–HA_{20} composite scaffolds after the selective extraction of the TZ, achieved by soaking the samples in a ethanol/water solution (90/10 v/v). The images evidenced a morphology characterized by an open macro-pore structure (as also observed for the initial scaffold morphologies, Fig. 3), interconnected to the smaller porosity induced by the extraction of the TZ phase (Fig. 7a and b). Furthermore, the resulting PCL and PCL–HA porous scaffolds were characterized by 60% overall porosities, sufficient for ensuring a structural support for cells and tissue even after the complete TZ degradation. Interestingly, the higher magnification of Fig. 7b also revealed that, for the PCL–TZ–HA_{20} scaffold, the large HA particles were partially crumbled during mixing, leading to a finer HA dispersion within the PCL matrix, with respect to original particles.

In order to assess the biocompatibility of the scaffolds, we performed two different *in vitro* cell culture tests, by using pre-osteoblast MG63 and hMSCs cells. Even if statically seeded, up to 75% of inoculated cells adhered to the scaffolds (data not shown). The SEM and CLSM analyses results reported in Fig. 8 confirmed the ability of the multi-phase scaffolds to allow for the adhesion and colonization of both cell types. In particular, the SEM image of the MG63 cell/scaffold construct at 1 day of culture, reported in Fig. 8a, showed that the cells adhered and colonized the pores of the scaffolds, also stretching and creating bridges between opposite pore walls (black arrows). Similarly, the CLSM results reported in Fig. 8b demonstrated that, at day 1 from seeding, the hMSCs were viable, adhering and colonizing the scaffold surface and, also following the topology of the pore walls. These results are in good agreement with those reported in the literature on the ability of both PCL and zein scaffolds to support cell adhesion and proliferation [9,10,20,30]. Furthermore, when blended with PCL, the TZ may improve the hydrophilic properties of the scaffolds and, therefore, the adsorption of the serum-derived ECM proteins responsible for cell adhesion and proliferation on biomaterial scaffolds [32].

4. Conclusions

In this study we prepared novel multi-phase porous scaffolds with fine controlled pore structures via $scCO_2$ foaming process. The optimization of materials formulation, mixing conditions and foaming parameters allowed for the control of the micro-structural properties and *in vitro* degradation of the scaffolds. In particular, the PCL–TZ and PCL–TZ–HA composite scaffolds prepared at $T_F = 100\ ^\circ C$ were characterized by porosity, pore size distribution and static compression properties suitable for bTE. The *in vitro* cell/scaffold interaction study also demonstrated that the proposed scaffolds allowed for the adhesion and colonization of pre-osteoblast MG63 and hMSCs cells.

Acknowledgements

The authors would like to thanks Maria Oliviero and Francesco Scavone for their support to this work.

References

[1] Hutmacher DW. Scaffolds in tissue engineering bone and cartilage. Biomaterials 2000;21(24):2529–43.
[2] Salgado AJ, Coutinho OP, Reis RL. Bone tissue engineering: state of the art and future trends. Macromol Biosci 2004;4(8):743–65.
[3] Burg KJL, Porter S, Kellam JF. Biomaterial developments for bone tissue engineering. Biomaterials 2000;21(23):2347–59.
[4] Petrie Aronin CE, Sadik KW, Lay AL, Rion DB, Tholpady SS, Ogle RC, et al. Comparative effects of scaffold pore size, pore volume, and total void volume on cranial bone healing patterns using microsphere-based scaffolds. J Biomed Mater Res Part A 2009;89(3):632–41.
[5] Leong KF, Chua CK, Sudarmadji N, Yeong WY. Engineering functionally graded tissue engineering scaffolds. J Mech Behav Biomed Mater 2008;S1:140–52.
[6] Karageorgiou V, Kaplan D. Porosity of 3D biomaterial scaffolds and osteogenesis. Biomaterials 2005;26(27):5474–91.
[7] Hollister SJ. Porous scaffold design for tissue engineering. Nature Mater 2005;4(7):518–24.
[8] Kim H, Knowles JC, Kim H. Hydroxyapatite and gelatin composite foams processed via novel freeze-drying and crosslinking for use as temporary hard tissue scaffolds. J Biomed Mater Res 2005;72A(2):136–45.
[9] Gong S, Wang H, Sun Q, Xue S, Wang J. Mechanical properties and in vitro biocompatibility of porous zein scaffolds. Biomaterials 2006;27(20):3793–9.
[10] Qu Z, Wang H, Tang T, Zhang X, Wang J, Dai K. Evaluation of the zein/inorganics composite on biocompatibility and osteoblastic differentiation. Acta Biomat 2008;4(5):1360–8.
[11] Kim S, Ahn K, Park MS, Lee J, Choi CY, Kim B. A poly(lactide-co-glycolide)/hydroxyapatite composite scaffold with enhanced osteoconductivity. J Biomed Mater Res 2007;80A(1):206–15.
[12] Murugan R, Ramakrishna S. Development of nanocomposites for bone grafting. Compos Sci Technol 2005;65(15–16):2385–406.
[13] She H, Xiao X, Liu R. Preparation and characterization of polycaprolactone–chitosan composites for tissue engineering applications. J Mater Sci 2007;42(19):8113–9.
[14] Rosa DS, Lopes DR, Calil MR. Thermal properties and enzymatic degradation of blends of poly(3-caprolactone) with starches. Polym Test 2005;24(6):756–61.
[15] Tu J, Wang H, Li H, Dai K, Wang J, Zhang X. The in vivo bone formation by mesenchymal stem cells in zein scaffolds. Biomaterials 2009;30(26):4369–76.
[16] Mathieu L, Bourban P, Månson J. Processing of homogeneous ceramic/polymer blends for bioresorbable composites. Compos Sci Technol 2006;66(11–12):1606–14.
[17] Tai H, Mather ML, Howard D, Wang W, White LJ, Crowe JA, et al. Control of pore size and structure of tissue engineering scaffolds produced by supercritical fluid processing. Eur Cells Mater 2007;14:64–77.
[18] Davies OR, Lewis AL, Whitaker MJ, Tai H, Shakesheff KM, Howdle SM. Applications of supercritical CO_2 in the fabrication of polymer systems for drug delivery and tissue engineering. Adv Drug Deliv Rev 2008;60(3):373–87.
[19] Ginty PJ, Howard D, Upton CE, Barry JJA, Rose FRAJ, Shakesheff KM, et al. A supercritical CO_2 injection system for the production of polymer/mammalian cell composites. J Supercr Fluids 2008;43(3):535–41.
[20] Salerno A, Oliviero M, Di Maio E, Iannace S, Netti PA. Design of porous polymeric scaffolds by gas foaming of heterogeneous blends. J Mater Sci: Mater Med 2009;20(10):2043–51.
[21] Salerno A, Oliviero M, Di Maio E, Iannace S. Thermoplastic foams from gelatin and zein. Int Polym Proc 2007;5:480–8.
[22] Joubert C, Cassagnau P, Michel A. Influence of the processing conditions on a two-phase reactive blend system: EVA/PP thermoplastic vulcanizate. Polym Eng Sci 2002;42(11):2222–33.
[23] Sessa DJ, Mohamed A, Byars JA. Chemistry and physical properties of melt-processed and solution-cross-linked corn zein. J Agric Food Chem 2008;56:7067–75.
[24] Mariani PDSC, Allganer K, Oliveira FB, Cardoso EJBN, Innocentini-Mei LH. Effect of soy protein isolate on the thermal, mechanical and morphological properties of poly(3-caprolactone) and corn starch blends. Polym Test 2009;28:824–9.
[25] Salerno A, Di Maio E, Iannace S, Netti PA. Engineering of foamed structures for biomedical applications. J Cell Plast 2009;45(2):103–17.
[26] Doroudiani S, Kortschot MT. Polystyrene foams. I. Processing–structure relationships. J Appl Polym Sci 2003;90(5):1412–20.
[27] Salerno A, Iannace S, Netti PA. Open-pore biodegradable foams prepared via gas foaming and microparticulate templating. Macromol Biosci 2008;8(7):655–64.
[28] Collins NJ, Leeke GA, Bridson RH, Hassan F, Grover LM. The influence of silica on pore diameter and distribution in PLA scaffolds produced using supercritical CO_2. J Mater Sci: Mater Med 2008;19(4):1497–502.

[29] Gibson LJ, Ashby MF. The mechanics of foams: basic results. In: Clarke DR, Suresh S, Ward IM, editors. Cellular solids. Cambridge; 1997. p. 175–217.
[30] Shor L, Güçeri S, Wen X, Gandhi M, Sun W. Fabrication of three-dimensional polycaprolactone/hydroxyapatite tissue scaffolds and osteoblast–scaffold interactions in vitro. Biomaterials 2007;28(35):5291–7.
[31] Yao C, Li X, Song T, Li Y, Pu Y. Biodegradable nanofibrous membrane of zein/silk fibroin by electrospinning. Polym Int 2009;58(4):396–402.
[32] Chastain SR, Kundu AK, Dhar S, Calvert JW, Putnam AJ. Adhesion of mesenchymal stem cells to polymer scaffolds occurs via distinct ECM ligands and controls their osteogenic differentiation. J Biom Mater Res Part A 2006;78A(1):73–85.